Efficient dual-wavelength excitation of Tb^{3+} emission in rare-earth doped KYF_4 cubic nanocrystals dispersed in silica sol-gel matrix

J. del-Castillo, A. C. Yanes, A. Santana-Alonso, J. Méndez-Ramos

Departamento de Física, Universidad de La Laguna, 38206 La Laguna, Tenerife, Spain

Abstract

Energy transfer from Ce^{3+} to Tb^{3+} ions under UV excitation, giving rise to visible emissions, is investigated in sol-gel derived transparent nano-glass-ceramics containing cubic KYF_4 nanocrystals, for different doping concentrations of rare-earth ions. Moreover, visible emissions of Tb^{3+} are also obtained under near-infrared excitation through energy transfer from Yb^{3+} ions by means of cooperative up-conversion processes. Thus, Ce^{3+}-Tb^{3+}-Yb^{3+} doped nano-glass-ceramics can be activated in a dual-wavelength mode yielding efficient blue-green emissions of particular interest in photovoltaic silicon solar cells and white-light emitting diodes.

Keywords: nano-glass-ceramics, rare-earth ions, sol-gel technique, up-conversion.

Introduction

The luminescence efficiency of rare-earth (RE) doped materials depends strongly on their local environments, responsible for multi-phonon decay rates, population of metastable energy levels, energy transfer (ET) and cross-relaxation (CR) processes [1,2]. Thus, low phonon energy hosts are desirable in order to avoid quenching intermediate energy levels. Fluorides exhibit low phonon energy when compared with oxides, which considerably reduces multi-phonon transitions, and so increasing the lifetime of excited RE doping ions. Others halides, i.e. chlorides, bromides, iodides, present lower phonon energy. However, RE ions exhibit lower Stark splitting, narrower excitation spectra and, consequently, a lower absorption from the ground to excited levels. Therefore, fluorides hosts become more suitable candidates for RE doping ions, since they favour long excited lifetimes and higher absorption cross-sections than other halides [3-5]. In addition, fluorides prevent the absorption band associated with the hydroxyl (OH) group (3200-3600 cm^{-1}) exhibited by most oxide based glasses, that can quench the luminescence of RE ions.

Oxyfluoride nano-glass-ceramics (nGCs) present the excellent optical properties of fluorides with a higher quantum efficiency, higher optical cross-section absorption, and good mechanical, electric, dielectric and magnetic properties than other reported hosts [3-7]. The advantages of these materials are based on the incorporation of RE ions into fluoride nanocrystals, with smaller size than the visible (VIS) wavelength, and refractive index similar to that of the surrounding glass matrix, and thus avoiding scattering losses [8]. Sol-gel derived nGCs can be obtained by an adequate heat-treatment of corresponding precursor glasses. The sol-gel technique presents some advantages to the conventional melting quenching methods [9], such as lower processing temperature, controllable composition, better chemical homogeneity, predetermined nanocrystals sizes and low cost of fabrication [10-13].

KYF_4 is well known as a suitable host for RE doping ions due to its low phonon energy favouring their optical properties by means of long lifetime of excited levels, high intensity of ultraviolet (UV) emissions [14], and high intense UV-VIS up-conversion (UC) emissions [15,16]. In particular, it can be found in the literature a few works concerning synthesis and optical properties of RE-doped KYF_4 cubic nanocrystals [17-20]. In this sense, the authors have recently reported highly efficient UC emissions and bright white light in this kind of hosts co-doped with Yb^{3+}-Tm^{3+}-Er^{3+}

[21], providing a remarkable higher efficiency in comparison with other fluoride hosts like $NaYF_4$ [22] and YF_3 [23]. The efficiency of emissions of lanthanide ions in this environment is favoured because they can occupy similar ionic radius Y^{3+} sites without need of charge compensation, increasing the solubility which is highly beneficial in down-conversion and UC processes.

Tb^{3+} presents a weak absorption cross-section in the UV and blue range, due to transitions 4f-4f are forbidden by the Laporte selection rule, only affected by a weak perturbation caused by the crystal field. On the contrary, Ce^{3+} ions present a large UV absorption cross-section due to the allowed 5d-4f electron transitions, and also a broad UV-blue emission band. Since this emission band overlaps with the absorption band of Tb^{3+}, it is possible to obtain blue and green emissions corresponding to 5d-4f transitions of Ce^{3+} and 4f-4f transitions of Tb^{3+}, respectively, under near UV excitation of 5d level of Ce^{3+} [24-32]. This down-shifting process is particularly interesting in photovoltaic applications by converting near UV solar radiation into VIS light where silicon solar cells work more efficiently and also in near-UV chips for white light emitting diodes (WLEDs).

Tb^{3+}-Yb^{3+} co-doped systems where NIR radiation can be obtained from UV or VIS light, by means of cooperative down-conversion by ET from Tb^{3+} to Yb^{3+} ions, can be found in the literature [33-35], since the energy of the transition $^5D_4 \rightarrow {}^7F_6$ of Tb^{3+} is approximately twice the energy of the transition $^2F_{7/2} \rightarrow {}^2F_{5/2}$ of Yb^{3+}. On the other side, the excited levels of Tb^{3+} can be populated at room temperature mainly through the UC process known as cooperative sensitization by means of ET from Yb^{3+} [36]. Thus, it has been recently obtained intense UC emissions in SrF_2 nanocrystals [37], in fluorogermanate glass-ceramics [38] and in aluminum silicate glass [39]. Additionally, the possibility of an excited state absorption (ESA) process, following the ET from Yb^{3+} ions, yielding to UC emissions of Tb^{3+} coming from $^5D_3$ level, has been reported. However, there is a lack of investigation on these RE-doped KYF_4 nGCs.

In this work, we investigate the luminescence properties and ET processes from Ce^{3+} to Tb^{3+} in cubic KYF_4 nGCs, as well as cooperative UC luminescence in Ce^{3+}-Tb^{3+}-Yb^{3+}, as an efficient dual-mode excitation pathway for Tb^{3+} blue-green emissions for potential applications in silicon solar cells and WLEDs.

Experimental

Silica glasses have been prepared by sol-gel method, as described in ref. [22], with following compositions: $95SiO_2$-$5KYF_4$ doped with xCe^{3+} where x = 0.1, 0.3 and 0.6, co-doped with $0.3Ce^{3+}$-yTb^{3+} where y = 0.1, 0.3, 0.5 and 1.0 and triply-doped with $0.3Ce^{3+}$-$0.5Tb^{3+}$-zYb^{3+} where z = 0.5 and 1.0 (mol %). Tetraethoxysilane (TEOS) $Si(OCH_2CH_3)_4$, used as a source of SiO_2, was hydrolyzed for 1 h at room temperature with a mixed solution of ethanol and deionised H_2O, using acetic acid as a catalyst. The molar ratio of TEOS:ethanol:H_2O:CH_3COOH was 1:4:10:0.5. As sources of Y and K, $Y(CH_3COO)_3 \cdot xH_2O$ and KCH_3COO were used. The required quantities of $Y(CH_3COO)_3 \cdot xH_2O$, KCH_3COO, $Ce(CH_3COO)_3 \cdot xH_2O$, $Tb(CH_3COO)_3 \cdot xH_2O$ and $Yb(CH_3COO)_3 \cdot xH_2O$ were dissolved in a CF_3COOH and H_2O solution, which was slowly mixed with the initial solution. The molar ratio of K^+, RE (Y^{3+}, Ce^{3+}, Tb^{3+}, Yb^{3+}) ions to CF_3COOH was 1:1:4. In order to obtain a homogeneous solution, the resultant one was stirred vigorously for 1 h at room temperature. A highly transparent gel was obtained by leaving the resultant homogeneous solution in a sealed container at 35 ºC for several days. Then, the gels were dried by a slow evaporation of the residual water and solvent. Finally, these sol-gel glasses were heat-treated in air at 650 °C in order to achieve a controlled precipitation of KYF_4 nanocrystals, giving rise to transparent nGCs. Moreover, $0.1Tb^{3+}$ single-doped nGC has been also prepared for comparison purposes.

X-ray powder diffraction (XRD) patterns of the samples were recorded with a Philips X'Pert Pro diffractometer equipped with a primary monochromator, Cu $K_{\alpha 12}$ radiation, and an X'Celerator detector. The XRD patterns were collected with a step of 0.016º in the 2θ angular range from 15 to 80º and an acquisition time of 2 h. Furthermore, the patterns were corrected by using LaB_6.

Luminescence measurements were obtained by exciting the samples with light from a 75 W Xe arc lamp passed through a 0.2 m monochromator (PTI spectrometer controlled by Felix32 software) and detecting with a 0.2 m monochromator with a R928 photomultiplier. Moreover, UC measurements were carried out with a 980 nm laser diode with pump power up to 250 mW, focused with a 50 mm lens, and detected through a 0.2 m monochromator equipped with a R928 photomultiplier. All spectra

were collected at room temperature and corrected by the instrumental response. CCD digital camera was used to take color pictures of luminescence emitted by the samples.

Results and Discussion

Structural characterization was carried out in terms of XRD. Thus, Fig.1 shows the XRD patterns of a precursor glass with composition $95SiO_2$-$5KYF_4$ triply-doped with 0.3 Ce^{3+}-0.5 Tb^{3+}-0.5Yb^{3+} (mol%) along with the corresponding nGC treated at 650 ºC. In the precursor sol-gel glass, only a broad band characteristic of an amorphous state is observed. However in the heat-treated sample, different diffraction peaks can be clearly distinguished located at 26.8, 30.7, 44.6 and 52.8º, which correspond to the precipitation of KYF_4 nanocrystals in the cubic phase (fluorite structures, space group *Fm-3m*) [17-20], no second crystalline phase was detected, in agreement with results reported in literature by H. Schäfer et al [20]. By using the Scherrer equation on the most intense peak (111) at 26.8º, radius around 7 nm is obtained. Similar XRD pattterns for the nGCs single doped with 0.3 Ce^{3+} and co-doped with 0.3 Ce^{3+}-0.5 Tb^{3+} were performed yielding similar nanocrystal radii. Transmission electron microscopy images of KYF_4 based-nano-glass-ceramics with similar composition have been already published by the authors [40] confirming the precipitation of KYF_4 nanoparticles, homogeneously dispersed in amorphous silica host matrix.

Excitation and emission spectra of *x*Ce^{3+} doped nGCs with increasing concentration (*x* = 0.1, 0.3, 0.6 mol %) are presented in Fig.2. The excitation spectra, obtained monitoring at the maximum of the corresponding emission bands for each concentration of Ce^{3+} ions, show that the intensity of the UV excitation band enhances when increasing the concentration of Ce^{3+} from 0.1 to 0.3 (mol %), while it is remarkably quenched for the 0.6 Ce^{3+} sample. Moreover, the maximum of the excitation bands is shifted to longer wavelengths when increasing the concentration of Ce^{3+}. On the other hand, the maximum of the emission spectra also presents a Stokes shifting when increasing the concentration of Ce^{3+}, maybe due in part to the fact that the allowed transition 4f-5d is sensitive to the environment and therefore experiment a higher crystal field [25,41] or to self-absorption concentration effects [42]. The emission spectra show an asymmetric band, with a single maximum which varies from 355 to 395 nm, which

could be related to overlap of multiple luminescent centers. It is clearly shown that the emission spectrum corresponding to a concentration of $0.3Ce^{3+}$ (mol %) exhibits the best overlapping with the excitation band of single Tb^{3+} doped nGCs, also shown in Fig.2. Thus, ET from Ce^{3+} to Tb^{3+} in co-doped nGCs could be optimized by using this concentration of Ce^{3+} due to the maximum of its emission band matches well with the excitation peaks of Tb^{3+} ions from 340 to 380 nm.

Figure 3 shows the emission spectra of $0.3Ce^{3+}$-$x Tb^{3+}$ (mol %) co-doped nGCs (x = 0.1, 0.3, 0.5, 1.0), exciting at the maximum of the UV Ce^{3+} excitation bands. Emissions have been labelled according to the energy level diagrams of Ce^{3+}, Tb^{3+} and Yb^{3+} ions shown in Fig.4. These emission spectra exhibit a shifting of the broad emission band of Ce^{3+} ions to lower wavelengths when increasing the concentration of Tb^{3+}. This can be related to the absorption contribution due to the overlapping of Tb^{3+} ions excitation peaks, corresponding to their electronic transitions depicted in the energy level diagram in Fig. 4. This absorption is obviously increased with Tb^{3+} concentration, yielding to the diminishment of the intensity of the corresponding long wavelength side of the Ce^{3+} emission, and therefore, to this apparent blue-shift of the maximum to lower wavelengths. These spectra also displays stronger emissions of Tb^{3+} in comparison with the broad emission band of Ce^{3+} when increasing the concentration of Tb^{3+}, indicating a more efficient ET process from Ce^{3+} to Tb^{3+}. These strong emissions, even for the lowest concentration of Ce^{3+}, (as it can be seen in the inset of Fig.3) indicate that Ce^{3+} is an excellent sensitizer for Tb^{3+} when both ions are co-doping a nGCs comprising KYF_4 nanocrystals. Further, the presence of high energy $^5D_3$ emissions of Tb^{3+} can be attributed to low CR processes between Tb^{3+} ions even at high concentrations. Additionally, these high energy emissions of Tb^{3+} may also be favoured by the low phonon energy of KYF_4, that avoids multiphonon relaxation processes, see energy level diagram in Fig.4.

Fig. 3 also presents an excitation spectrum of the $0.3Ce^{3+}$- $0.5Tb^{3+}$ co-doped nGCs monitoring at the maximum emission peak of Tb^{3+} located at 543 nm, showing an intense excitation band in the UV attributed to the transition $4f^8 \rightarrow 4f^7 5d$ of Ce^{3+} ions, along with direct weaker excitation peaks of Tb^{3+} ions, confirming a very efficient ET from Ce^{3+} to Tb^{3+}. Moreover, a similar UV excitation band is observed when detecting at the maximum of the Ce^{3+} emission band (not shown in Fig.3), similar to the

previously depicted for $0.3Ce^{3+}$ single-doped nGCs in Fig.2, confirming the Ce^{3+}-related origin of this UV band.

The color coordinates corresponding to the total VIS emissions of these spectra are shown in the CIE diagram in Fig. 5. It can be observed that the nGCs single-doped with Ce^{3+} emits only in the blue, corresponding to its transition 5d → 4f. On the other hand, in the co-doped nGCs, the ET from Ce^{3+} to Tb^{3+} involves a progressive shifting of the color emission mainly to the greenish, when exciting Ce^{3+} ions at the UV band and increasing the concentration of Tb^{3+}, mainly due to its intense emission $^5D_4 \rightarrow {}^7F_5$.

Fig. 6 presents emission spectra of $0.3Ce^{3+}$-$0.5Tb^{3+}$ co-doped nGCs, showing a shift to longer wavelengths of the broad emission of Ce^{3+} ions, along with a broadening of the emission peaks of Tb^{3+} ions, with increasing excitation wavelength, as it can be observed in the figure. These features suggest an ET from Ce^{3+} to Tb^{3+} ions in different environments: mainly inner KYF_4 nanocrystals sites and at the near-surfaces, as it will be discussed next. Moreover, a detailed study of the two components of the $^5D_4 \rightarrow {}^7F_5$ transition of Tb^{3+} ions can be also related with different environments for RE^{3+} ions. Thus, by exciting at the maximum of the UV Ce^{3+} excitation band, at 290 nm, the green main emission presents only one component centered at 543 nm that is also observed in the up-conversion spectra that will be analyzed next. Whereas, when exciting at higher wavelengths, i.e. 320 nm, two components clearly appear at 543 and 550 nm, that can be related with the presence of Tb^{3+} ions near or in the SiO_2-KYF_4 interface. These two components also appear in the typical emission spectrum of a SiO_2:Tb^{3+} sol-gel glass, see right inset of Fig.6, supporting this assumption.

Moreover, it should be noticed their corresponding color coordinates in the CIE diagram, see left inset in Fig.6, allowing the possibility of tuning the overall emitting color, from greenish to bluish part, as a function of different excitation wavelengths in the UV range, yielding a wide color gamut that would satisfy technological requirements for WLEDs applications.

On the other hand, the normalized emission spectra corresponding to a $0.3Ce^{3+}$ single-doped nGCs exciting at different wavelengths along the UV Ce^{3+} excitation band, are also presented in Fig.6. It can be noticed a shift to longer wavelengths of the emission band of Ce^{3+} as a function of the excitation wavelength, from 290 to 320 nm, similar to the observed behaviour for the Ce^{3+}-Tb^{3+} co-doped samples, as was

previously discussed, confirming the existence of different environments for RE^{3+} ions, inside or near the KYF_4 nanocrystals [43].

Moreover, to discern between these different environments, time-resolved photoluminescence measurements were carried out. In particular, the evolution of the luminescent decay from the $^5D_4$ level of Tb^{3+} ions was measured selecting the excitation and detection wavelengths, which correspond to different sites previously observed. Thus, Fig.7 shows luminescence decays for $0.3Ce^{3+}$-$0.5Tb^{3+}$ co-doped nGCs, exciting at 290 nm and monitoring the 543 nm emission (corresponding to a nanocrystalline KYF_4 environment and exciting at 320 nm and monitoring the 550 nm emission (corresponding to near to the KYF_4 nanoparticle surface site). The increase of decay time from 3.0 to 4.3 ms is obtained when going from interface SiO_2-KYF_4 to those Tb^{3+} ions partitioned into KYF_4 nanocrystals. Besides, a shorter decay time of 2.5 ms for $^5D_4$ level of Tb^{3+} ions in a SiO_2 glass doped with Tb^{3+} previously published by the authors [44], supports the assumption of the interface environment with slightly longer decay time.

Fig. 8 presents the luminescence features of the Ce^{3+}-Tb^{3+}-Yb^{3+} triply-doped nGCs. UC emission spectra of $0.3Ce^{3+}$-$0.5Tb^{3+}$-$x$$Yb^{3+}$ (mol %) nGCs, where x = 0.5 and 1.0, under 980 nm excitation, point out to cooperative UC processes by ET from Yb^{3+} to Tb^{3+} ions, as indicated in the energy level diagram in Fig. 4. It should be noticed that increasing the concentration of Yb^{3+} causes, on one hand, an enhancement of the absorption of the NIR pumping photons and, on the other hand, favours cooperative UC processes among Yb^{3+} pairs. Moreover, these spectra show intense UC emissions coming from $^5D_3$ level, which is probably populated by ESA/ET from $^5D_4$ level [45]. These high energy emissions from $^5D_3$ are favoured with increasing the Yb^{3+} concentration as can be clearly seen in the Fig.8. Moreover, the emission spectrum of the nGCs triply-doped with $0.3Ce^{3+}$-$0.5Tb^{3+}$-$0.5Yb^{3+}$ (mol %) exciting at the Ce^{3+} UV band is also presented in Fig. 8, showing similar features to the $0.3Ce^{3+}$-$0.5Tb^{3+}$ co-doped nGCs and moreover, main Tb^{3+} emissions from $^5D_4$ level show similar features to the corresponding ones appearing in the UC emission spectra presented above. ~~Therefore, as conclusion, the main Tb^{3+} emissions in these Ce^{3+}-Tb^{3+}-Yb^{3+} triply-doped nGCs can be excited in a dual-wavelength mode with potential applications in enhanced response silicon solar cells and WLEDs~~.

Conclusions

Sol-gel derived transparent nGCs containing cubic KYF_4 nanocrystals have been successfully synthesized and characterized by XRD patterns. ET processes from Ce^{3+} to Tb^{3+} ions under UV excitation, yielding blue-green emissions, were studied as a function of different doping concentration and excitation wavelengths, by analysing luminescence spectra. Besides, cooperative up-conversion processes also give rise to efficient blue-green emissions of Tb^{3+} ions under NIR. Therefore, dual-wavelength excitation, i.e, both under NIR and UV pump, has been achieved in the Ce^{3+}-Tb^{3+}-Yb^{3+} triply-doped nGCs, giving rise to these Tb^{3+} ions visible emissions, which can be useful for increasing the spectral response of silicon photovoltaic cells and also in the WLEDs research field.

Acknowledgments

The authors would like to thank Fundación CajaCanarias (NAFOWLEDs) and Ministerio de Ciencia y Tecnología of Spain Government (MAT2009-12079) for financial support.

References

[1] C.K. Jorgensen, R. Reisfeld, Top. Curr. Chem. 147 (1982).

[2] R. Reisfeld, C.K. Jorgensen, Handbook on the Physics and Chemistry of Rare Earths, North Holland, Amsterdam (1987).

[3] M. Shojiya, M. Takahashi, R. Kanno, Y. Kawamoto, K. Kadono, Appl. Phys. Lett. 67, 2453 (1995).

[4] H. U. Gudel , M. Pollnau, J. Alloys Compd. 303, 307 (2000).

[5] F. Wang, X. Liu, Chem. Soc. Rev. 38, 976 (2009).

[6] H. Gleiter, Acta Mater. 48, 1 (2000).

[7] C. Suryanarayana, B. Mater. Sci. 17, 307 (1994).

[8] M. Mortier, A. Monteville, G. Patriarche, G. Maze, F. Auzel, Opt. Mater. 15, 255 (2001).

[9] S. Fujihara, C. Mochizuki, T. Kimura, J. Non-Cryst. Solids 244, 267 (1999).

[10] A. Biswas, G.S. Maciel, R. Kapoor, C.S. Friend, P.N. Prasad, Appl. Phys. Lett. 82, 2389 (2003).

[11] S.J.L. Ribeiro, C.C. Araújo, L.A. Burno, R.R. Goncalves, Y. Messaddeq, J. Non-Cryst. Solids 348, 180 (2004).

[12] C.J. Brinker, G.W. Scherer, Sol-Gel Science: The Physics and Chemistry of Sol-Gel Processing, Academic, San Diego (1990).
[13] R. Morimo, K. Matae, Mater. Res. Bull. 24, 175 (1989).
[14] N.M. Khaidukov, M. Kirm, S.K. Lam, D. Lo, V.N. Makhov, G. Zimmerer, Opt. Commun. 184, 183 (2000).
[15] L. Bonelli, A. Toncelli, A.D. Lieto, M. Tonelli, J. Phys. Chem. Solids 68, 2381 (2007).
[16] T.R. Park, T.Y. Park, S.H. Youn, N.M. Khaidukov, J. Lumin. 106, 281 (2004).
[17] H. Schäfer, P. Ptacek, K. Hickmann, M. Prinz, M. Neumann, M. Haase, Russ. J. Inorg. Chem. 54, 1914 (2009).
[18] Y. Wang, Y. Liu, Q. Xiao, H. Zhu, R. Li, X. Chen, Nanoscale 3, 3164 (2011).
[19] Y.P. Du, Y.W. Zhang, L.D. Sun, C.H. Yan, Dalton Trans. 8574 (2009).
[20] H. Schäfer, P. Ptacek, O. Zerzouf, M. Haase, Adv. Funct. Mater. 18, 2913 (2008).
[21] J. Méndez-Ramos, A.C. Yanes, A. Santana-Alonso, J. del-Castillo, Chem. Phys. Lett. 555, 196 (2013).
[22] J. Méndez-Ramos, A.C. Yanes, A. Santana-Alonso, J. del-Castillo, V.D. Rodríguez, J. Nanosci. Nanotechno. 10, 1273 (2010).
[23] A.C. Yanes, A. Santana-Alonso, J. Méndez-Ramos, J. del-Castillo, V.D. Rodríguez, Adv. Funct. Mater. 21, 3136 (2011).
[24] J. Sun, Y. Sun, J. Lai, Z. Xia, H. Du, J. Lumin. 132, 3048 (2012).
[25] Q. Luo, X. Qiao, X. Fan, X. Zhang, J. Non-Cryst. Solids 356, 2875 (2010).
[26] X.M. Zhang, W.L. Li, K.H. Jang, H.J. Seo, Curr. Appl. Phys. 12, 299 (2012).
[27] B. Wang, L. Sun, H. Ju, Solid State Commun. 150, 1460 (2010).
[28] J. Zheng, C. Guo, X. Ding, Z. Ren, J. Bai, Curr. Appl. Phys. 12, 643 (2012).
[29] J.J. Velázquez, V.D. Rodríguez, A.C. Yanes, J. del-Castillo, J. Méndez-Ramos, Opt. Mater. 34, 1994 (2012).
[30] G. Li, S. Lana, L. Li, M. Li, W. Baoa, H. Zoua, X. Xub, S. Gana, J. Alloys Compd. 513, 145 (2012).
[31] K.G. Tshabalala, S.H. Cho, J.K. Park, S.S. Pitalea, I.M. Nagpure, R.E. Kroon, H.C. Swart, O.M. Ntwaeaborwa, Physica B 407, 1489 (2012).
[32] Y. Li, X. Wei, M. Yin, Y. Tao, Opt. Mater. 33, 1239 (2011).
[33] S. Ye, Y. Katayama, S. Tanabe, J. Non-Cryst. Solids 357, 2268 (2011).
[34] S. Ye, B. Zhu, J. Chen, J. Luo, J. R. Qiu, Appl. Phys. Lett. 92, 141112 (2008).
[35] Y. Wang, L. Xie, H. Zhang, J. Appl. Phys. 105, 023528 (2009).

[36] G.M. Salleya, R. Valienteb, H.U. Guedela, J. Lumin. 94, 305 (2001).

[37] X. Qiao, X. Fan, Z. Xue, X. Xu, Q. Luo, J. Lumin. 131, 2036 (2011).

[38] A.S. Gouveia-Neto, L.A. Bueno, A.C.M. Afonso, J.F. Nascimento, E.B. Costa, Y. Messaddeq, S.J.L. Ribeiro, J. Non-Cryst. Solids 354, 509 (2008).

[39] R.K. Verma, D.K. Rai, S.B. Rai, J. Alloys Compd. 509, 5591 (2011).

[40] A.C. Yanes, A. Santana-Alonso, J. Méndez-Ramos, J. del-Castillo. Appl. Phys. B 113, 589 (2013).

[41] P. Thiyagarajan, B. Tiwari, M. Kottaisamy, N. Rama, M.S. Ramachandra Rao, Appl. Phys. A 94, 607 (2009).

[42] L. Fachun, B. Lijing, Y. Zhiping, L. Quanlin. J of Rare Earths 30, 851 (2012).

[43] Y. Wang, Y. Liu, Q, Xiao, H. Zhu, R. Li, X. Chen, Nanoscale 3, 3164 (2011).

[44] J.J. Velázquez, V.D. Rodríguez, A.C. Yanes, J. del-Castillo, J. Méndez-Ramos, J. Appl. Phys. 108, 1, (2010).

[45] F. Xin, S. Zhao, G. Jia, L. Huang, D. Deng, H. Wang, S. Xu. Mat. Chem. Phys. 137, 177 (2013).

Figure captions

Fig.1. XRD patterns of as-made sample and nGC heat treated at 650 ºC triply doped with $0.3Ce^{3+}$-$0.5Tb^{3+}$-$0.5Yb^{3+}$.

Fig. 2. Excitation (solid) and emission (dash) spectra of $x Ce^{3+}$ single-doped nGCs, where x = 0.1, 0.3 and 0.6 (mol %), monitoring and exciting at the maximum of the corresponding bands, along with an excitation spectrum of $0.1Tb^{3+}$ single-doped nGCs detecting at 543 nm.

Fig. 3. Emission spectra of $0.3Ce^{3+}$-xTb^{3+} co-doped nGCs, where x = 0.1, 0.3, 0.5 and 1.0 (mol %), exciting at the maximum of Ce^{3+} excitation band. Spectra are normalized at the maximum of the $^5D_4 \rightarrow {}^7F_5$ transition of Tb^{3+} ions. Excitation spectrum of $0.3Ce^{3+}$-$0.5Tb^{3+}$ nGC monitoring at 543 nm. Inset shows emission spectrum of $0.1Ce^{3+}$-$1.0Tb^{3+}$ co-doped nGCs, exciting at the maximum of Ce^{3+} excitation band.

Fig. 4. Energy level diagrams of Ce^{3+}, Tb^{3+} and Yb^{3+} ions.

Fig. 5. Color coordinates in the CIE standard chromaticity diagram of $0.3Ce^{3+}$-xTb^{3+} co-doped nGCs, where x = 0, 0.1, 0.3, 0.5 and 1.0 (mol %), under UV excitation at the maximum of the excitation band of Ce^{3+}, around 300 nm. Photographs of the different samples under UV excitation are also included.

Fig. 6. (a) Emission spectra of $0.3Ce^{3+}$-$0.5Tb^{3+}$ (mol %) co-doped nGCs, exciting at indicated wavelengths and normalized at the maximum of the $^5D_4 \rightarrow {}^7F_5$ transition of Tb^{3+} ions. (b) Emission spectra of $0.3Ce^{3+}$ single-doped nGCs (mol %), exciting at indicated wavelengths and normalized at the maximum. Right inset shows emission spectrum of a SiO_2-$4\%Tb^{3+}$ sol-gel glass, exciting at 350 nm. Left inset presents CIE color coordinates of $0.3Ce^{3+}$-$0.5Tb^{3+}$ (mol %) nGCs, under different UV excitations.

Fig. 7. Time-resolved luminescence decay curves of nGCs co-doped with $0.5Tb^{3+}$-$0.3Ce^{3+}$ (mol %), exciting at 290 and monitoring at 543 nm emission (filled circle) and exciting at 320 and monitoring at 550 nm emission (opened square).

Fig. 8. UC emission spectra of nGCs co-doped with $0.3Ce^{3+}$-$0.5Tb^{3+}$-xYb^{3+} (mol %), where x = 0.5 and 1.0, under 980 nm excitation at 250 mW, along with direct emission spectrum of the $0.3Ce^{3+}$-$0.5Tb^{3+}$-$0.5Yb^{3+}$ nGCs (mol %), exciting at the maximum of Ce^{3+} UV band.

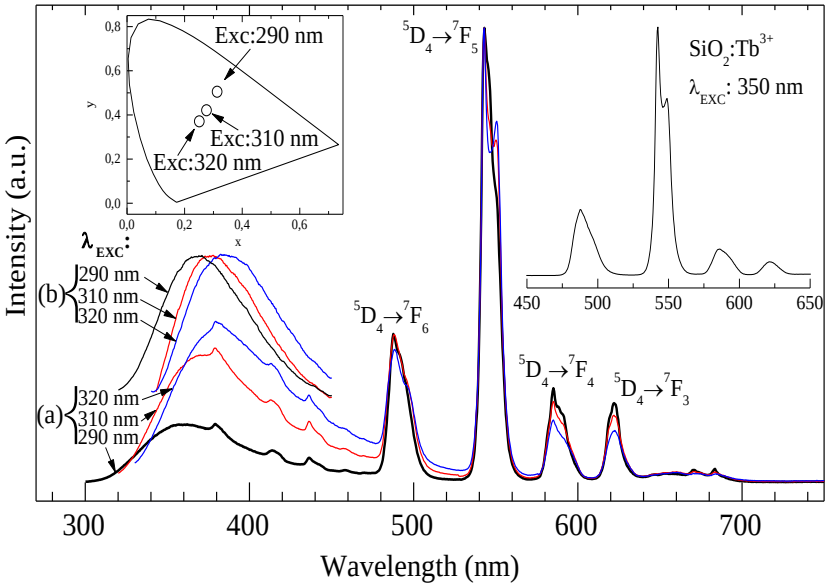
Intensity (a.u.)
Wavelength (nm)
300
400
500
600
700
$^5D_4 \rightarrow ^7F_5$
$^5D_4 \rightarrow ^7F_6$
$^5D_4 \rightarrow ^7F_4$
$^5D_4 \rightarrow ^7F_3$
$SiO_2:Tb^{3+}$
λ_{EXC}: 350 nm
450
500
550
600
650
Exc:290 nm
Exc:310 nm
Exc:320 nm
x
y
0,0
0,2
0,4
0,6
0,8
λ_{EXC}:
(b)
290 nm
310 nm
320 nm
(a)
320 nm
310 nm
290 nm

Fig. 6.

Figure

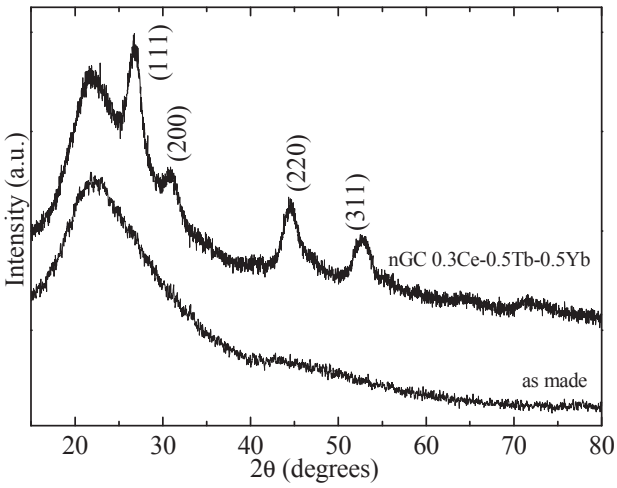
Intensity (a.u.)
(111)
(200)
(220)
(311)
nGC 0.3Ce-0.5Tb-0.5Yb
as made
20
30
40
50
60
70
80
2θ (degrees)

Fig. 1.

Figure

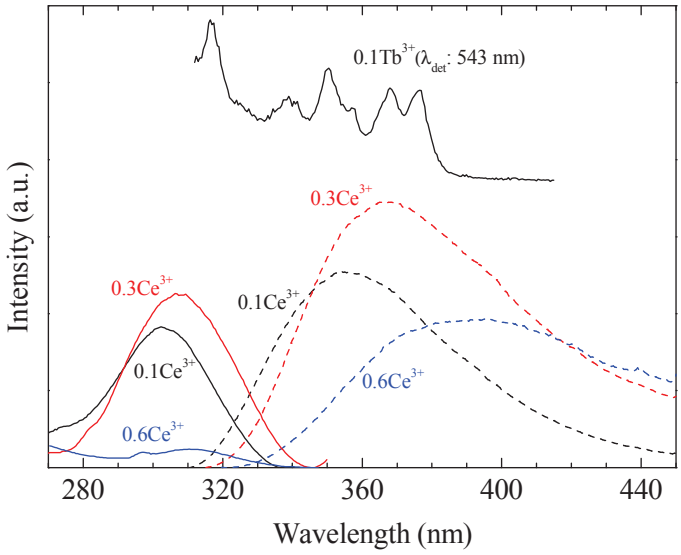
0.1Tb3+(λdet: 543 nm)
0.3Ce3+
0.3Ce3+
0.1Ce3+
0.1Ce3+
0.6Ce3+
0.6Ce3+
Intensity (a.u.)
280
320
360
400
440
Wavelength (nm)

Fig.2

Figure

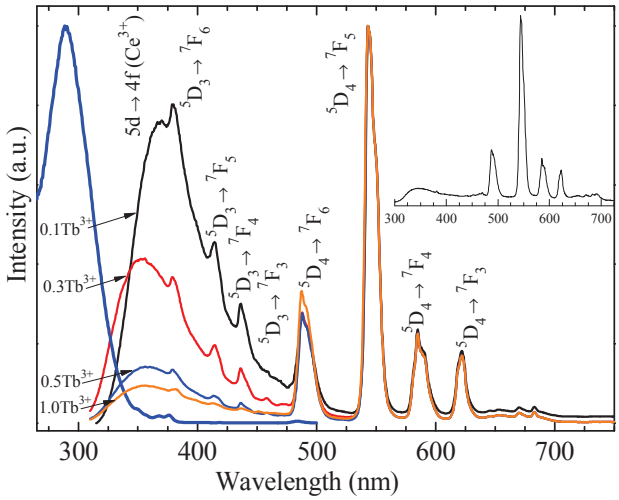
Intensity (a.u.)
Wavelength (nm)
300
400
500
600
700
5d → 4f (Ce3+)
5D3 → 7F6
5D3 → 7F5
5D3 → 7F4
5D3 → 7F3
5D4 → 7F6
5D4 → 7F5
5D4 → 7F4
5D4 → 7F3
0.1Tb3+
0.3Tb3+
0.5Tb3+
1.0Tb3+

Fig. 3.

Figure

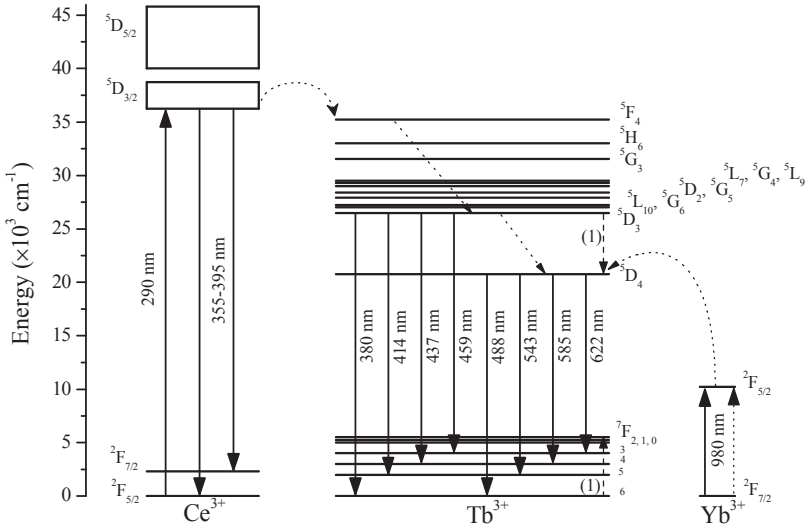
Energy (×10^3 cm^-1)
45
40
35
30
25
20
15
10
5
0
5D5/2
5D3/2
290 nm
355-395 nm
2F7/2
2F5/2
Ce3+
5F4
5H6
5G3
5L10, 5G6, 5D2, 5G5, 5L7, 5G4, 5L9
5D3
(1)
5D4
380 nm
414 nm
437 nm
459 nm
488 nm
543 nm
585 nm
622 nm
7F2, 1, 0
3
4
5
6
(1)
Tb3+
2F5/2
980 nm
2F7/2
Yb3+

Fig. 4.

Figure

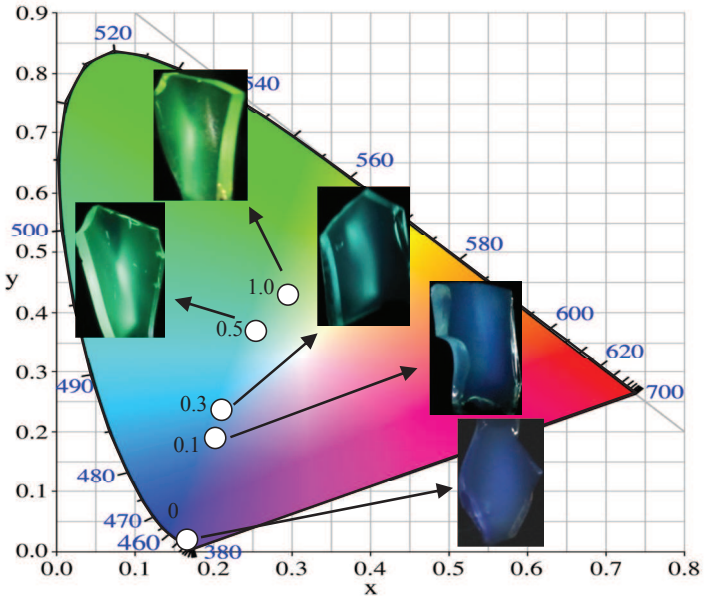
0.9
0.8
0.7
0.6
0.5
0.4
0.3
0.2
0.1
0.0
y
0.0
0.1
0.2
0.3
0.4
0.5
0.6
0.7
0.8
x
520
540
560
580
600
620
700
500
490
480
470
460
380
1.0
0.5
0.3
0.1
0

Fig. 5

Figure

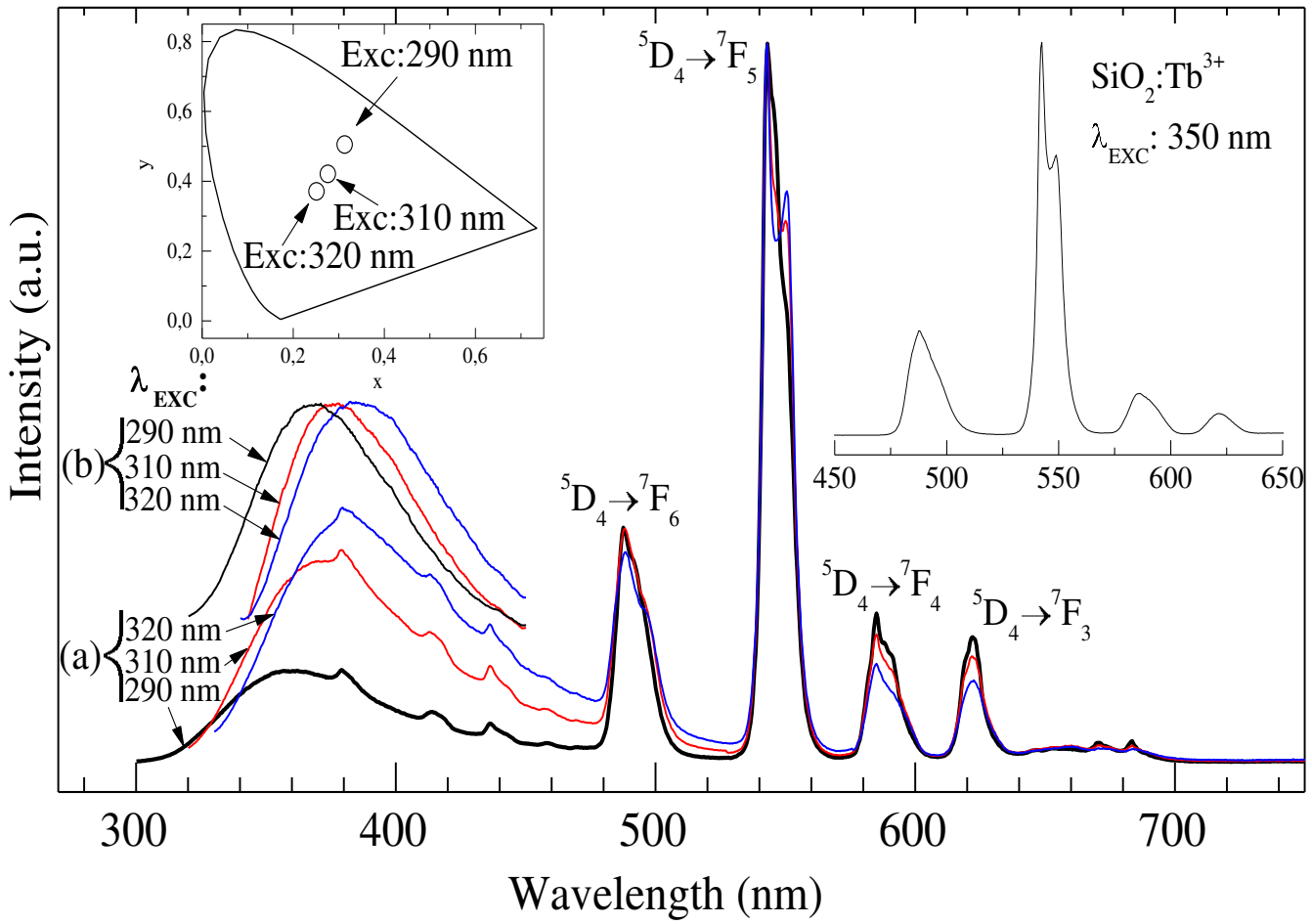
Intensity (a.u.)
Wavelength (nm)
300
400
500
600
700
$^5D_4 \rightarrow {}^7F_5$
$^5D_4 \rightarrow {}^7F_6$
$^5D_4 \rightarrow {}^7F_4$
$^5D_4 \rightarrow {}^7F_3$
$SiO_2:Tb^{3+}$
λ_{EXC}: 350 nm
450
500
550
600
650
λ_{EXC}:
(b)
290 nm
310 nm
320 nm
(a)
320 nm
310 nm
290 nm
Exc:290 nm
Exc:310 nm
Exc:320 nm
0,0
0,2
0,4
0,6
0,8
x
y

Fig. 6.

Figure

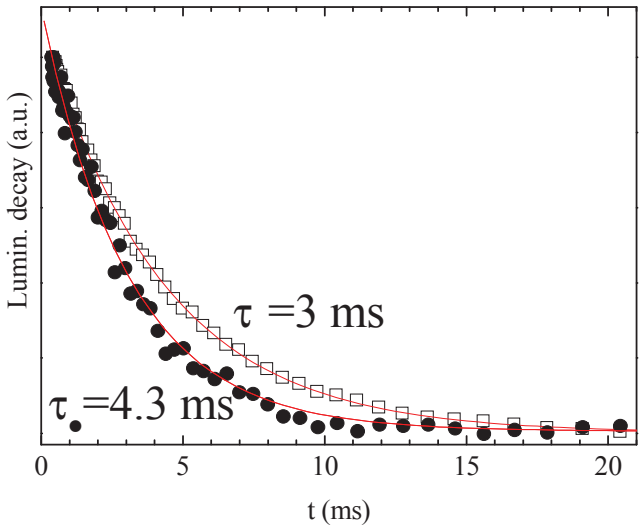

Fig. 7.

Figure

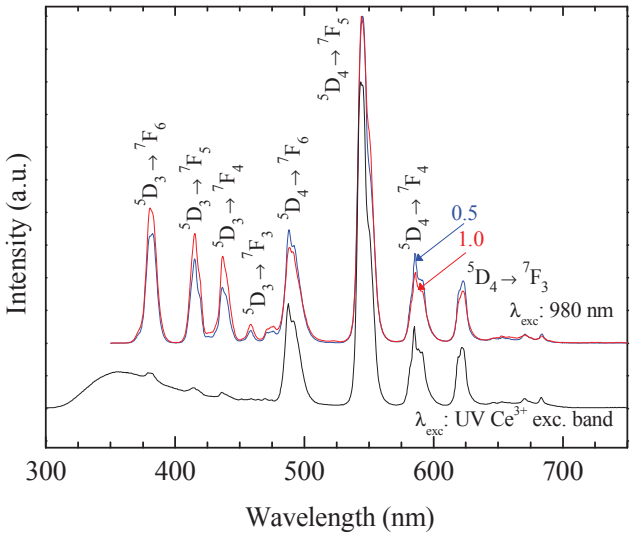
Intensity (a.u.)
Wavelength (nm)
300
400
500
600
700
$^5D_3 \rightarrow {}^7F_6$
$^5D_3 \rightarrow {}^7F_5$
$^5D_3 \rightarrow {}^7F_4$
$^5D_3 \rightarrow {}^7F_3$
$^5D_4 \rightarrow {}^7F_6$
$^5D_4 \rightarrow {}^7F_5$
$^5D_4 \rightarrow {}^7F_4$
$^5D_4 \rightarrow {}^7F_3$
0.5
1.0
λ_{exc}: 980 nm
λ_{exc}: UV Ce^{3+} exc. band

Fig. 8.